2019

Non-linear tyre model-based non-singular terminal sliding mode observer for vehicle velocity and side-slip angle estimation

Boyuan Li
University of Wollongong

Haiping Du
University of Wollongong, hdu@uow.edu.au

Weihua Li
University of Wollongong, weihuali@uow.edu.au

Bangji Zhang
Hunan University, bangjizhang@hnu.edu.cn

Non-linear tyre model-based non-singular terminal sliding mode observer for vehicle velocity and side-slip angle estimation

Abstract

Vehicle velocity and side-slip angle are important vehicle states for the electronic stability programme and traction control system in vehicle safety control system and for the control allocation method of electric vehicles with in-wheel motors. This paper proposes an innovative side-slip angle estimator based on the non-linear Dugoff tyre model and non-singular terminal sliding mode observer. The proposed estimation method based on the non-linear tyre model can accurately present the tyre's non-linear characteristics and can show advantages over estimation methods based on the linear tyre model. The utilised Dugoff tyre model has a relatively simple structure with few parameters, and the proposed non-linear observer can be applied in various vehicle tyres and various road conditions. Precise determination of the Dugoff tyre model parameters is not required and the proposed observer can still perform good estimation results even though tyre parameters and the tyre-road friction coefficient are not accurate. The proposed non-singular terminal sliding mode observer can achieve fast convergence rate and better estimation performance than the traditional sliding mode observer. At the end of this paper, simulations in various conditions are presented to validate the proposed non-linear estimator.

Disciplines

Engineering | Science and Technology Studies

Publication Details

B. Li, H. Du, W. Li & B. Zhang, "Non-linear tyre model-based non-singular terminal sliding mode observer for vehicle velocity and side-slip angle estimation," Proceedings of the Institution of Mechanical Engineers, Part D: Journal of Automobile Engineering, vol. 233, (1) pp. 38-54, 2019.

Non-linear tyre model based non-singular terminal sliding mode observer for vehicle velocity and side-slip angle estimation

Boyuan Li[1,2], Haiping Du[2*], Weihua Li[3] and Bangji Zhang[1]

1. State Key Laboratory of Advanced Design and Manufacturing for Vehicle Body, Hunan University, Changsha 410082, China

2. School of Electrical, Computer and Telecommunications Engineering, University of Wollongong, Wollongong, NSW 2522, Australia

3. School of Mechanical, Material and Mechatronic Engineering, University of Wollongong, Wollongong, NSW 2522, Australia

*Corresponding author, email address: hdu@uow.edu.au

Abstract:

Vehicle velocity and side-slip angle are important vehicle states for the electronic stability program (ESP) and traction control system (TCS) in vehicle safety control system and for the control allocation method of electric vehicles with in-wheel motors. This paper proposes an innovative side-slip angle estimator based on the non-linear Dugoff tyre model and non-singular terminal sliding mode observer (NS-TSMO). The proposed estimation method based on the non-linear tyre model, can accurately present the tyre's non-linear characteristics and can show advantages over estimation methods based on the linear tyre model. The utilised Dugoff tyre model has a relatively simple structure with few parameters, and the proposed non-linear observer can be applied in

various vehicle tyres and various road conditions. Precise determination of the Dugoff tyre model parameters is not required and the proposed observer can still perform good estimation results even though tyre parameters and the tyre-road friction coefficient are not accurate. The proposed NS-TSMO observer can achieve fast convergence rate and better estimation performance than the traditional SMO observer. At the end of this paper, simulations in various conditions are presented to validate the proposed non-linear estimator.

Key words: **side-slip angle estimation, Dugoff tyre model, sliding mode method**

I. INTRODUCTION

Nowadays, due to the increased population and traffic congestion in modern cities, traffic accidents have become the major issue for on-road vehicles. The electronic stability program (ESP) and traction control system (TCS) in the vehicle safety control system can significantly improve road safety and reduce road accidents [1]. The active front wheel steering (AFS) and direct yaw moment control (DYC) are integrated together to achieve a human-machine-cooperative-driving control (HMCDC) [2]. These control systems, however, usually require the measurement of longitudinal velocity, lateral velocity and yaw rate. In general conditions, yaw rate is measurable but obtaining the accurate vehicle velocities is a challenging task due to cost and reliability.

In order to successfully estimate the vehicle velocities, various model-based estimation methods based on vehicle dynamics model are proposed in the literature [3] [4] [5].

Electrified vehicles have attracted wide attention due to their usage of clean energy, fast and accurate system responses and various easy-to-implement dynamic controllers and trajectory controllers. Especially for electric vehicles with in-wheel motors, the over-actuated control allocation method is applied to control the vehicle dynamics such as handling and stability [6] [7]. The most important vehicle state value to determine the stability of the vehicle is the vehicle body side-slip angle, so the feedback information of actual side-slip angle is critical for the stability control system. Thus, the estimation of side-slip angle plays an important role for the stability control of electrified vehicles or particularly electric vehicles with in-wheel motors.

The estimation of vehicle velocities is closely related to the estimation of body side-slip angle, since the body side-slip angle β can be calculated by the following equation:

$$\beta = \tan^{-1}\left(\frac{v_y}{v_x}\right) \tag{1}$$

where v_x is the vehicle longitudinal velocity and v_y is the vehicle lateral velocity. Thus, the velocity estimation sometimes is presented as the body side-slip angle estimation in the literature.

Various vehicle velocity (body side-slip angle) estimation methods exist in the literature, such as the Kalman filter method, sliding mode method, and intelligent algorithm method. Kalman filter based estimation method is a widely applied velocity estimation method. A side-slip angle observer which combined the direct integration method with the Kalman filter was proposed in [5]. Some studies applied the Extended Kalman filter (EKF) method to estimate the vehicle velocity and friction forces [8] [9] and an EKF-like observer was also presented in [10] to estimate the side-slip angle. In [11], a novel EKF estimation method for the side-slip angle and roll angle estimation is proposed. This EKF estimation method includes a fusion algorithm which introduces the direct integration of the measured side-slip angle rate to compensate the side-slip angle estimated by EKF and improve the estimation performance. The EKF method can deal with the non-linear characteristic of dynamics model by using Taylor expansion approximation and is advantageous to tackle the process noise and measurement noise with Gauss distribution. Some studies proposed some modified EKFs to improve the estimation performance when tyre or vehicle parameters are inaccurate, such as the adaptive EKF [12], variable structure EKF [3] and identifying EFK [13]. An innovative adaptive square-root cubature Kalman filter (ASCKF) based estimator is proposed in [14] and the integral correction fusion algorithm is proposed to compensate the estimation error caused by the unknown coloured sensor noise. On the other hand, sliding mode technique is also widely utilised to design the vehicle velocity estimator.

A robust $H\infty$ sliding mode observer (SMO) was designed to estimate the vehicle body side-slip angle subject to the exogenous disturbances, unknown inputs and uncertain measurements [15]. Zhang and Wang also designed a finite-frequency mixed $H_-/H\infty$ gain-scheduling observer in [16]. Stèphant designed a SMO to estimate the body side-slip angle [17]. In this study, the linear tyre friction force model is used, but the linear tyre model is not accurate enough to present the non-linear tyre friction characteristics. Zhao et al. utilised the non-linear Dugoff tyre model and comprehensive vehicle dynamics model as the plant to accurately present the vehicle motion and provide the measurement information of accelerations and yaw rate, but the proposed observer is still simple linear observer [18]. For the intelligent algorithm method, Huang proposed the neural network algorithm [19] and Shi applied the fuzzy logic method to estimate side-slip angle [20]. For the other methods, Zhang et al. utilised the real experimental electric vehicle to collect the measurement signals, such as velocity and yaw rate, and to identify important parameters of the vehicle lateral dynamics model [21]. Then based on this lateral dynamics model, a model-based state observer is proposed by finite-frequency H_∞ approach. This study uses experimental data to identify the parameters of lateral tyre friction model, but the accuracy of the identified parameters is questionable if the vehicle tyre property or the vehicle moving condition is changing.

In the above discussed literature, the linear model-based observer for the vehicle state and side-slip angle estimation is widely used, while there is less application of the non-

linear tyre model into the side-slip angle observer. Furthermore, the side-slip angle estimation method based on sliding mode technique is more reliable than EKF method and intelligent algorithm method.

In the current literature, the non-linear tyre friction model can be classified as the empirical tyre model and physical tyre model. A widely used empirical tyre model is Magic formula tyre model, which is easy to implement due to its simple structure and fewer parameters. However, the tyre parameters strongly rely on the curve-fitting results of experimental tyre data and may not be accurate if the tyre data is changed [22]. On the other hand, two typical physical tyre models are LuGre tyre model proposed by Deur et al. [23] and brush tyre model proposed in [24]. Physical tyre models can accurately present the tyre physical properties without relying on the curve-fitting results of the tyre force data, but the major disadvantage of this kind of tyre model is its complex structure including too many tyre physical parameters, which makes it hard to implement. Dugoff tyre model, a simpler tyre model dating back to 1970 [25], is a semi-empirical non-linear tyre model and can present the physical property of the tyre using a few parameters, such as longitudinal (lateral) tyre cornering stiffness, vertical load and friction coefficient. The Dugoff tyre model is advantageous because of its simplified structure and ease of implementation. More importantly, this tyre model can be used to present various vehicle tyres under various road conditions by simply adjusting the cornering stiffness and tyre-road friction coefficient. Therefore, the Dugoff tyre model

has been widely applied to present non-linear tyre characteristics [26] [18] [27] [28]. In the current literature, the non-linear Magic formula tyre model and non-linear Fiala tyre model (similar to brush tyre model) have been widely applied for the side-slip angle estimation. Ma et al. applied the non-linear Magic formula tyre model to design the EKF for the side-slip angle estimation [29]. Li and Zhang presented a new hybrid Kalman filter to estimate the vehicle side-slip angle based on the 3 DOF vehicle dynamics model combined with the non-linear Magic formula tyre model [30]. Hsu et al. utilised the pneumatic trail information in steering torque based on non-linear Fiala tyre model to identify a vehicle's lateral handling limits and side-slip angle [31] [32]. However, the application of non-linear Dugoff tyre model into vehicle side-slip angle estimation has received less attention. Although the non-linear Dugoff-based vehicle dynamics model was utilised to obtain the measured feedback vehicle states in [18], the observer proposed was still a linear observer. In [33], a simplified Dugoff tyre model which neglected the tyre longitudinal slip was applied to design an EKF side-slip angle estimator, but the simplified Dugoff tyre model could not fully present the tyre’s non-linear characteristics.

The sliding mode method has been widely applied for the estimation and dynamic control of the vehicle system. However, the conventional SMC laws are discontinuous and can cause the well-known chattering phenomenon. To overcome this drawback, various techniques have been employed, such as boundary layer approach [34], reaching

law approach [35] and self-turning sliding mode [36]. Alipour et al. suggested the proportional-integral sliding mode control (PISMC) strategy to improve the fault-tolerant control performance of the traditional SMC so that a smaller control gain could be selected and the chattering effect could be reduced [37]. The sliding surface of conventional SMC is usually described as linear switching functions, while the so-called 'terminal sliding model control' (TSMC) applies the non-linear switching manifolds to achieve fast and finite-time convergence and eliminate the chattering phenomenon. The non-singular terminal sliding mode technique was employed in [38] and the reaching law was designed by including the negative exponential factor, which could not only guarantee the finite-time convergence of the system states, but also overcome the singularity problem associated with the conventional TSMC. However, few of the current studies have integrated the NS-TSMO into the vehicle side-slip angle estimator.

In our proposed estimator in this paper, the non-singular terminal SMO (NS-TSMO) based on the non-linear comprehensive vehicle dynamics model is proposed for the side-slip angle estimation. This estimation method incorporates the non-linear Dugoff tyre model into the SMO to accurately present the non-linear tyre characteristic. The major contribution of this study can be summarised as follows: 1) the non-linear Dugoff tyre model has been incorporated into the vehicle side-slip angle observer to present better tyre non-linear characteristics than linear tyre model; 2) the NS-TSMO technique

is also applied in the side-slip angle observer to achieve faster and better finite-time convergence of the estimation values than traditional SMO; 3) the proposed non-linear NS-TSMO also shows robustness when tyre parameters in the estimator are not accurate and the road condition is changing.

The rest of this paper is organised as follows. Vehicle non-linear modelling for the observer design is presented in Section 2. The simple SMO based on linear tyre model and NS-TSMO based on non-linear Dugoff tyre model are shown in Section 3. The simulation results of comparing the linear model method and non-linear method are shown in Section 4. Finally, the conclusion is given in Section 5.

II. VEHICLE DYNAMICS MODEL

Vehicle body model

In this paper, in order to develop the non-linear side-slip angle estimator, the comprehensive vehicle dynamics model is proposed in this section [26], which is shown in Figure 1. The equations of motion of this model are described as follows:

Longitudinal motion:

$$m\dot{v}_x = mv_y r + \left(F_{xfl} + F_{xfr} + F_{xrl} + F_{xrr}\right)$$

(2)

Lateral motion:

$$m\dot{v}_y = -mv_x r + \left(F_{yfl} + F_{yfr} + F_{yrl} + F_{yrr}\right)$$

(3)

Yaw motion:

$$I_z\dot{r} = l_f\left(F_{yfl} + F_{yfr}\right) - l_r\left(F_{yrl} + F_{yrr}\right) + \frac{b_f}{2}\left(F_{xfl} - F_{xfr}\right) + \frac{b_r}{2}\left(F_{xrl} - F_{xrr}\right)$$

(4)

where v_x, v_y, r are the vehicle longitudinal velocity, lateral velocity, and yaw rate, respectively. $F_{xfl}, F_{xfr}, F_{xrl}, F_{xrr}$ are the vehicle front left, front right, rear left and rear right longitudinal tyre forces, respectively, and $F_{yfl}, F_{yfr}, F_{yrl}, F_{yrr}$ are the vehicle front left, front right, rear left and rear right lateral tyre forces, respectively. l_f and l_r are the front and rear wheel base lengths, while b_f and b_r are the front and rear track widths. I_z and m are the moment of vehicle inertia in terms of yaw axis and vehicle mass. The vehicle roll dynamics and pitch dynamics are neglected for simplicity but the actual

lateral and longitudinal load transfer are included in the vehicle model as shown equation (9) in a quasi-static manner.

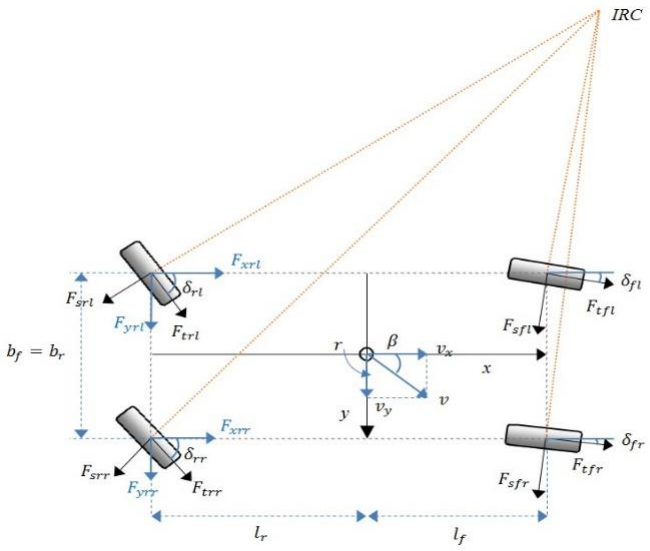

Figure 1. 4WIS-4WID vehicle dynamics model, where IRC represents the instantaneous centre of rotation.

The tyre traction or brake force and side force are defined as F_{ti} and F_{si}, respectively, which can be related to the longitudinal and the lateral tyre forces by the steering angle δ_i as follows:

$$F_{xi} = F_{ti}\cos\delta_i - F_{si}\sin\delta_i$$

$$F_{yi} = F_{ti}\sin\delta_i + F_{si}\cos\delta_i \tag{5}$$

where $i = fl, fr, rl, rr$, which represents the front left, front right, rear left and rear right wheel, respectively.

Combing equations (2)-(5), the dynamic model of the vehicle can be rewritten as:

$$\begin{bmatrix} \dot{v}_x \\ \dot{v}_y \\ \dot{r} \end{bmatrix} = \begin{bmatrix} v_y r \\ -v_x r \\ 0 \end{bmatrix} + B_y(\delta_i)\boldsymbol{F_s} + B_x(\delta_i)\boldsymbol{F_t} \tag{6}$$

where $\boldsymbol{F_t} = [F_{tfl} \quad F_{tfr} \quad F_{trl} \quad F_{trr}]^{\boldsymbol{T}}$, $\boldsymbol{F_s} = [F_{sfl} \quad F_{sfr} \quad F_{srl} \quad F_{srr}]^{\boldsymbol{T}}$, which presents the tyre force along the wheel direction (the tractive force) and perpendicular to the wheel direction (the side force), respectively.

$B_x(\delta_i)$

$$= \begin{bmatrix} \frac{1}{m} & 0 & 0 \\ 0 & \frac{1}{m} & 0 \\ 0 & 0 & \frac{1}{I_z} \end{bmatrix} \begin{bmatrix} \cos\delta_{fl} & \cos\delta_{fr} & \cos\delta_{rl} & \cos\delta_{rr} \\ \sin\delta_{fl} & \sin\delta_{fr} & \sin\delta_{rl} & \sin\delta_{rr} \\ l_f \sin\delta_{fl} + \frac{b_f}{2}\cos\delta_{fl} & l_f \sin\delta_{fr} - \frac{b_f}{2}\cos\delta_{fr} & \frac{b_r}{2}\cos\delta_{rl} - l_r \sin\delta_{rl} & -\frac{b_r}{2}\cos\delta_{rr} - l_r \sin\delta_{rr} \end{bmatrix}$$

$$= \begin{bmatrix} B_{x1} \\ B_{x2} \\ B_{x3} \end{bmatrix}$$

$$B_y(\delta_i)$$

$$= \begin{bmatrix} \frac{1}{m} & 0 & 0 \\ 0 & \frac{1}{m} & 0 \\ 0 & 0 & \frac{1}{I_z} \end{bmatrix} \begin{bmatrix} -\sin\delta_{fl} & -\sin\delta_{fr} & -\sin\delta_{rl} & -\sin\delta_{rr} \\ \cos\delta_{fl} & \cos\delta_{fr} & \cos\delta_{rl} & \cos\delta_{rr} \\ l_f\cos\delta_{fl} - \frac{b_f}{2}\sin\delta_{fl} & l_f\cos\delta_{fr} + \frac{b_f}{2}\sin\delta_{fr} & -\frac{b_r}{2}\sin\delta_{rl} - l_r\cos\delta_{rl} & \frac{b_r}{2}\sin\delta_{rr} - l_r\cos\delta_{rr} \end{bmatrix}$$

$$= \begin{bmatrix} B_{y1} \\ B_{y2} \\ B_{y3} \end{bmatrix}$$

Vehicle tyre model

The non-linear Dugoff tyre model, which can well describe the non-linear tyre characteristic of combined longitudinal and lateral tyre force and the friction circle effect [25], is described by:

$$\lambda_i = \frac{\mu F_{zi}\left[1 - \varepsilon_r u_i \sqrt{s_i^2 + \tan^2\alpha_i}\right](1 - s_i)}{2\sqrt{C_s^2 s_i^2 + C_\alpha^2 \tan^2\alpha_i}}$$

$$f(\lambda_i) = \begin{cases} \lambda_i(2 - \lambda_i) & (\lambda_i < 1) \\ 1 & (\lambda_i > 1) \end{cases}$$

$$F_{si} = \frac{C_\alpha \tan\alpha_i}{1 - s_i} f(\lambda_i)$$

$$F_{ti} = \frac{C_s s_i}{1 - s_i} f(\lambda_i)$$

(7)

where μ is the tyre-road friction coefficient. C_s is the longitudinal cornering stiffness and C_α is the lateral cornering stiffness. Figure 2 presents the curve of vehicle lateral tyre force versus different side-slip angles under different tyre cornering stiffness values, which suggests the tyre force is greatly affect by tyre parameters. s_i is the longitudinal slip ratio, and α_i is the lateral slip angle.ε_r is a constant value, and u_i is the vehicle velocity component in the wheel plane which is defined for each wheel as:

$$u_{fl} = \left(v_x + \frac{1}{2} b_f r\right) \cos \delta_{fl} + \left(v_y + l_f r\right) \sin \delta_{fl}$$

$$u_{fr} = \left(v_x - \frac{1}{2} b_f r\right) \cos \delta_{fr} + \left(v_y + l_f r\right) \sin \delta_{fr}$$

$$u_{rl} = \left(v_x + \frac{1}{2} b_r r\right) \cos \delta_{rl} - \left(l_r r - v_y\right) \sin \delta_{rl}$$

$$u_{rl} = \left(v_x - \frac{1}{2} b_r r\right) \cos \delta_{rr} - \left(l_r r - v_y\right) \sin \delta_{rr}$$

(8)

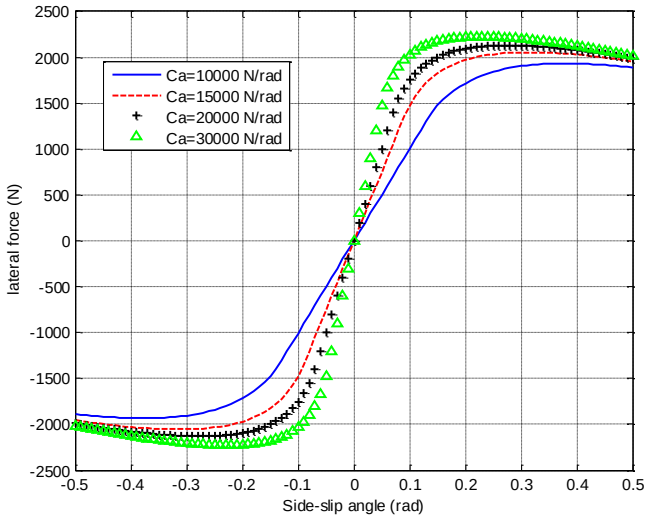

Figure 2. The vehicle lateral tyre force corresponding to different side-slip angles under different tyre cornering stiffness values ($v_x = 100km/h$)

F_{zi} is the vertical load of each wheel, which can be calculated as follows [39]:

$$F_{zfl} = \frac{m}{l_f + l_r}\left(\frac{1}{2}gl_r - \frac{1}{2}\dot{v}_x h - \frac{l_r}{b_f}\dot{v}_y h\right)$$

$$F_{zfr} = \frac{m}{l_f + l_r}\left(\frac{1}{2}gl_r - \frac{1}{2}\dot{v}_x h + \frac{l_r}{b_f}\dot{v}_y h\right)$$

$$F_{zrl} = \frac{m}{l_f + l_r}\left(\frac{1}{2}gl_f + \frac{1}{2}\dot{v}_x h - \frac{l_f}{b_r}\dot{v}_y h\right)$$

$$F_{zrl} = \frac{m}{l_f + l_r}\left(\frac{1}{2}gl_f + \frac{1}{2}\dot{v}_x h + \frac{l_f}{b_r}\dot{v}_y h\right)$$

(9)

where h is the height of the vehicle CG above the ground.

Traction or brake dynamics model

The wheel rotation dynamics is described by the following equation:

$$I_\omega \dot{\omega}_i = -R_\omega F_{ti} + T_i \tag{10}$$

where I_ω is the wheel moment of inertia and ω_i is the angular velocity of each wheel. R_ω is the wheel radius and T_i is the traction or brake torque of each wheel.

III. SIDE-SLIP ANGLE SLIDING MODE OBSERVER (SMO)

In this section, the simple linear tyre model based sliding mode observer (SMO) is presented first and then the proposed NS-TSMO based on the non-linear Dugoff tyre model is described. It is assumed that the available measurement inputs are longitudinal acceleration, lateral acceleration, steering angle, wheel speed and yaw rate. This assumption is reasonable since the vehicle acceleration can be measured by the inertial

measurement unit (IMU) or accelerometer, and the wheel speed and yaw rate are both easy to measure.

Simple SMO based on the linear tyre model

The linear tyre model simplified the relationship between the longitudinal tyre force (lateral tyre force) and longitudinal slip ratio (lateral side-slip angle) as the longitudinal cornering stiffness (the lateral cornering stiffness):

$$F_{si} = C_\alpha \alpha_i \tag{11a}$$

$$F_{ti} = C_s s_i \tag{11b}$$

The simple SMO based on the linear tyre model can be designed as the follows:

$$\begin{bmatrix} \hat{v}_x \\ \hat{v}_y \\ \hat{r} \end{bmatrix} = \begin{bmatrix} \hat{v}_y \hat{r} \\ -\hat{v}_x \hat{r} \\ 0 \end{bmatrix} + B_y(\delta_i)\widehat{\boldsymbol{F}}_{\boldsymbol{s}} + B_x(\delta_i)\widehat{\boldsymbol{F}}_{\boldsymbol{t}} + \boldsymbol{V} \tag{12}$$

where $\boldsymbol{V} = \begin{bmatrix} v_1 \\ v_2 \\ v_3 \end{bmatrix}$. v_1, v_2, v_3 represent the sliding mode observer law. $\hat{v}_x$, $\hat{v}_y$, $\hat{r}$ represent the estimated longitudinal velocity, lateral velocity and yaw rate. $\widehat{\boldsymbol{F}}_{\boldsymbol{t}}$ and $\widehat{\boldsymbol{F}}_{\boldsymbol{s}}$ represent the estimated values of tractive force and side force, which can be calculated as follows:

$$\hat{F}_t = C_s \hat{s}_i = C_s \frac{\omega_i R_\omega - \hat{v}_x}{max(\hat{v}_x, \omega_i R_\omega)} \tag{13}$$

$$\hat{F}_{sfl} = C_a \hat{a}_{fl} = C_a \left[\delta_{fl} - atan\left(\frac{\hat{v}_y + l_f \hat{r}}{\hat{v}_x - \frac{1}{2} b_f \hat{r}} \right) \right] \tag{14a}$$

$$\hat{F}_{sfr} = C_a \hat{a}_{fr} = C_a \left[\delta_{fr} - atan\left(\frac{\hat{v}_y + l_f \hat{r}}{\hat{v}_x + \frac{1}{2} b_f \hat{r}} \right) \right] \tag{14b}$$

$$\hat{F}_{srl} = C_a \hat{a}_{rl} = C_a \left[\delta_{rl} + atan\left(\frac{l_r \hat{r} - \hat{v}_y}{\hat{v}_x - \frac{1}{2} b_r \hat{r}} \right) \right] \tag{14c}$$

$$\hat{F}_{srr} = C_a \hat{a}_{rr} = C_a \left[\delta_{rl} + atan\left(\frac{l_r \hat{r} - \hat{v}_y}{\hat{v}_x + \frac{1}{2} b_r \hat{r}} \right) \right] \tag{14d}$$

where $\hat{s}_i$ and $\hat{a}_i$ are the estimated longitudinal slip ratio and lateral side-slip angle, respectively.

The estimation error can be calculated by subtracting equation (6) from (12):

$$\dot{\tilde{v}}_x = \left(\tilde{v}_y r + \hat{v}_y \tilde{r} \right) + B_{y1}(\delta_i) \widetilde{\boldsymbol{F}}_{\boldsymbol{s}} + B_{x1}(\delta_i) \widetilde{\boldsymbol{F}}_{\boldsymbol{t}} + v_1 \tag{15a}$$

$$\dot{\tilde{v}}_y = -(\tilde{v}_x r + \hat{v}_x \tilde{r}) + B_{y2}(\delta_i) \widetilde{\boldsymbol{F}}_{\boldsymbol{s}} + B_{x2}(\delta_i) \widetilde{\boldsymbol{F}}_{\boldsymbol{t}} + v_2 \tag{15b}$$

$$\dot{\tilde{r}} = B_{y3}(\delta_i) \widetilde{\boldsymbol{F}}_{\boldsymbol{s}} + B_{x3}(\delta_i) \widetilde{\boldsymbol{F}}_{\boldsymbol{t}} + v_3 \tag{15c}$$

where $\tilde{v}_x = \hat{v}_x - v_x$, $\tilde{v}_y = \hat{v}_y - v_y$, $\widetilde{\boldsymbol{F}}_{\boldsymbol{t}} = \widehat{\boldsymbol{F}}_{\boldsymbol{t}} - \boldsymbol{F}_{\boldsymbol{t}}$ and $\widetilde{\boldsymbol{F}}_{\boldsymbol{s}} = \widehat{\boldsymbol{F}}_{\boldsymbol{s}} - \boldsymbol{F}_{\boldsymbol{s}}$.

The sliding surface of the SMO can be selected as follows:

$$S_1 = \int \tilde{a}_x \tag{16a}$$

$$S_2 = \int \tilde{a}_y \tag{16b}$$

$$S_3 = \tilde{r} \tag{16c}$$

where $\tilde{a}_x = \hat{a}_x - a_x$,which represents the error between the estimated longitudinal acceleration and actual value. $\tilde{a}_y = \hat{a}_y - a_y$, which represents the error between the estimated lateral acceleration and actual value. $a_x = B_{y1}(\delta_i)\boldsymbol{F_s} + B_{x1}(\delta_i)\boldsymbol{F_t}$, $a_y = B_{y2}(\delta_i)\boldsymbol{F_s} + B_{x2}(\delta_i)\boldsymbol{F_t}$, $\dot{r} = B_{y3}(\delta_i)\boldsymbol{F_s} + B_{x3}(\delta_i)\boldsymbol{F_t}$. $\tilde{r} = \hat{r} - r$.

The time derivative of the sliding surface of the SMO can be calculated as:

$$\dot{S}_1 = \tilde{a}_x = \dot{\tilde{v}}_x - \left(\tilde{v}_y r + \hat{v}_y \tilde{r}\right) - v_1 \tag{17a}$$

$$\dot{S}_2 = \tilde{a}_y = \dot{\tilde{v}}_y + (\tilde{v}_x r + \hat{v}_x \tilde{r}) - v_2 \tag{17b}$$

$$\dot{S}_3 = \dot{\tilde{r}} + v_3 \tag{17c}$$

Thus, the observer law $\boldsymbol{V}$ can be determined as follows:

$$v_1 = (\hat{a}_x - a_x) + k_1 sgn(S_1) \tag{18a}$$

$$v_2 = \left(\hat{a}_y - a_y\right) + k_2 sgn(S_2) \tag{18b}$$

$$v_3 = -\dot{\tilde{r}} - k_3 sgn(S_3) \tag{18c}$$

According to equations (12) and (18), the linear observer requires the measured information of longitudinal acceleration, lateral acceleration, input steering angle, wheel angular velocity and yaw rate.

To prove the stability of the suggested control law, the Lyapunov method is used. The Lyapunov functions for the three channels can be chosen as:

$$V_1 = \frac{1}{2}S_1^2 \tag{19a}$$

$$V_2 = \frac{1}{2}S_2^2 \tag{19b}$$

$$V_3 = \frac{1}{2}S_3^2 \tag{19c}$$

The time derivative of the above Lyapunov function is:

$$\dot{V}_1 = S_1\dot{S}_1 = S_1\left[\dot{\tilde{v}}_x - \left(\tilde{v}_y r + \hat{v}_y\tilde{r}\right) - v_1\right] = -k_1|S_1| \tag{20a}$$

$$\dot{V}_2 = S_2\dot{S}_2 = S_2\left[\dot{\tilde{v}}_y + \left(\tilde{v}_x r + \hat{v}_x\tilde{r}\right) - v_2\right] = -k_2|S_2| \tag{20b}$$

$$\dot{V}_3 = S_3\dot{S}_3 = S_3\left(\dot{\tilde{r}} + v_3\right) = -k_3|S_3| \tag{20c}$$

According to equation (20), the time derivative of the above Lyapunov function is always negative, which proves the stability of the whole system.

Non-linear Dugoff tyre model based NS-TSMO

Similarly, according to equation (6), the proposed *NS-TSMO* can be designed as equation (12). Compared with the above linear method, the estimated tyre force in equation (12) can be determined by non-linear Dugoff tyre model:

$$\hat{F}_{si} = \frac{C_\alpha \tan \hat{\alpha}_i(\hat{v}_x,\hat{v}_y,\hat{r},\delta_i)}{1-\hat{s}_i(\hat{v}_x,\omega_i)} f\left(\lambda_i(\hat{\alpha}_i, \hat{s}_i, \mu, F_{zi})\right) \tag{21a}$$

$$\hat{F}_{ti} = \frac{C_s \hat{s}_i(\hat{v}_x,\omega_i)}{1-\hat{s}_i(\hat{v}_x,\omega_i)} f\left(\lambda_i(\hat{\alpha}_i, \hat{s}_i, \mu, F_{zi})\right) \tag{21b}$$

The estimation error dynamics equation (15) can be obtained by subtracting equation (6) from equation (12).

In order to obtain the terminal convergence of the tracking error, the sliding surface can be defined as:

$$s_1 = \int \int \tilde{a}_x + \frac{1}{\beta_1}(\int \tilde{a}_x)^{\frac{p_1}{q_1}} \tag{22a}$$

$$s_2 = \int \int \tilde{a}_y + \frac{1}{\beta_2}\left(\int \tilde{a}_y\right)^{\frac{p_2}{q_2}} \tag{22b}$$

$$s_3 = \int \tilde{r} + \frac{1}{\beta_3}\tilde{r}^{\,p_3/q_3} \tag{22c}$$

where $\beta_1, \beta_2, \beta_3 \in R^+$, $p_1, p_2, p_3, q_1, q_2, q_3$ are positive odd integrators. The time derivatives of the sliding surfaces s_1, s_2, s_3 defined by (22) are derived as following equations:

$$\dot{s}_1 = \int \tilde{a}_x + \frac{p_1}{\beta_1 q_1}\left(\int \tilde{a}_x\right)^{\frac{p_1}{q_1}-1} \tilde{a}_x$$

$$= \int \tilde{a}_x + \frac{p_1}{\beta_1 q_1}\left(\int \tilde{a}_x\right)^{\frac{p_1}{q_1}-1} \left[\dot{\tilde{v}}_x - \left(\tilde{v}_y r + \hat{v}_y \tilde{r}\right) - v_1\right]$$

$$= \int \tilde{a}_x - \frac{p_1}{\beta_1 q_1}\left(\int \tilde{a}_x\right)^{\frac{p_1}{q_1}-1} v_1 + \frac{p_1}{\beta_1 q_1}\left(\int \tilde{a}_x\right)^{\frac{p_1}{q_1}-1} \left[\dot{\tilde{v}}_x - \left(\tilde{v}_y r + \hat{v}_y \tilde{r}\right)\right]$$

(23a)

$$\dot{s}_2 = \int \tilde{a}_y + \frac{p_2}{\beta_2 q_2}\left(\int \tilde{a}_y\right)^{\frac{p_2}{q_2}-1} \tilde{a}_y = \int \tilde{a}_y + \frac{p_2}{\beta_2 q_2}\left(\int \tilde{a}_y\right)^{\frac{p_2}{q_2}-1} \left[\dot{\tilde{v}}_y + \left(\tilde{v}_x r + \hat{v}_x \tilde{r}\right) - v_2\right]$$

$$= \int \tilde{a}_y - \frac{p_2}{\beta_2 q_2}\left(\int \tilde{a}_y\right)^{\frac{p_2}{q_2}-1} v_2 + \frac{p_2}{\beta_2 q_2}\left(\int \tilde{a}_y\right)^{\frac{p_2}{q_2}-1} \left[\dot{\tilde{v}}_y + \left(\tilde{v}_x r + \hat{v}_x \tilde{r}\right)\right]$$

(23b)

$$\dot{s}_3 = \tilde{r} + \frac{p_3}{\beta_3 q_3} \tilde{r}^{p_3/q_3 - 1} \dot{\tilde{r}} = \tilde{r} + \frac{p_3}{\beta_3 q_3} \tilde{r}^{p_3/q_3 - 1} \left(\dot{\hat{r}} - \dot{r} + \boldsymbol{v_3}\right)$$

$$= \tilde{r} + \frac{p_3}{\beta_3 q_3} \tilde{r}^{p_3/q_3 - 1} v_3 + \frac{p_3}{\beta_3 q_3} \tilde{r}^{p_3/q_3 - 1} \left(\dot{\tilde{r}}\right)$$

(23c)

In order to guarantee the sliding reaching law is designed by employing an attractor with the negative exponential factor, the observer law $\boldsymbol{V} = \begin{bmatrix} v_1 \\ v_2 \\ v_3 \end{bmatrix}$ can be designed as:

$$v_1 = \frac{\beta_1 q_1}{p_1}\left(\int \tilde{a}_x\right)^{2-\frac{p_1}{q_1}} + \frac{\beta_1 q_1}{p_1}\left(k_1 s_1 + r_1 s_1^{\,m_1/n_1}\right)$$

(24a)

$$v_2 = \frac{\beta_2 q_2}{p_2}\left(\int \tilde{a}_y\right)^{2-\frac{p_2}{q_2}} + \frac{\beta_2 q_2}{p_2}\left(k_2 s_2 + r_2 s_2^{\,m_2/n_2}\right)$$

(24b)

$$v_3 = -\frac{\beta_3 q_3}{p_3}\tilde{r}^{\,2-\frac{p_3}{q_3}} - \frac{\beta_3 q_3}{p_3}\left(k_3 s_3 + r_3 s_3^{\,m_3/n_3}\right)$$

(24c)

Substituting equation (24) into (23):

$$\dot{s}_1 = -\left(k_1 s_1 + r_1 s_1^{\,m_1/n_1}\right)\left(\int \tilde{a}_x\right)^{\frac{p_1}{q_1}-1} + \frac{p_1}{\beta_1 q_1}\left(\int \tilde{a}_x\right)^{\frac{p_1}{q_1}-1}\left[\dot{\tilde{v}}_x - \left(\tilde{v}_y r + \hat{v}_y \tilde{r}\right)\right]$$

(25a)

$$\dot{s}_2 = -\left(k_2 s_2 + r_2 s_2^{\,m_2/n_2}\right)\left(\int \tilde{a}_y\right)^{\frac{p_2}{q_2}-1} + \frac{p_2}{\beta_2 q_2}\left(\int \tilde{a}_y\right)^{\frac{p_2}{q_2}-1}\left[\dot{\tilde{v}}_y + (\tilde{v}_x r + \hat{v}_x \tilde{r})\right]$$

(25b)

$$\dot{s}_3 = -\left(k_3 s_3 + r_3 s_3^{\,m_3/n_3}\right)\tilde{r}^{\,p_3/q_3-1} + \frac{p_3}{\beta_3 q_3}\tilde{r}^{\,p_3/q_3-1}\left(\dot{\tilde{r}}\right)$$

(25c)

Assumption 1 The constants $\beta_i > 0, k_i > 0, r_i > 0$ and the positive odd integrators m_i, n_i, p_i, q_i satisfy the constraints: $0 < m_i < n_i < 1$, $1 < m_i < n_i < 2$, where $i = 1,2,3$. The observer gain $r_i > 0$ and $k_i > 0$ and satisfying:

$$k_1 > \left|\frac{c_1}{s_1}\right| \tag{26a}$$

$$k_2 > \left|\frac{c_2}{s_2}\right| \tag{26b}$$

$$k_3 > \left|\frac{c_3}{s_3}\right| \tag{26c}$$

Assumption 2 The tyre model errors ΔF_x and ΔF_y are bounded and satisfy the following condition:

$$B_{y1}(\delta_i)\boldsymbol{F_s} + B_{x1}(\delta_i)\boldsymbol{F_t} \leq c_1$$

(27a)

$$B_{y2}(\delta_i)\boldsymbol{F_s} + B_{x2}(\delta_i)\boldsymbol{F_t} \leq c_2 \tag{27b}$$

$$B_{y3}(\delta_i)\boldsymbol{F_s} + B_{x3}(\delta_i)\boldsymbol{F_t} \leq c_3 \tag{27c}$$

where c_1, c_2 and c_3 are positive constant values.

Theorem 1 Consider the vehicle non-linear dynamic system (2)-(10) and the proposed non-linear SMO (12) with the observer law (24). When assumption 1 and assumption 2 are satisfied, the tracking errors of observer (12) converge asymptotically to zero in finite time.

The detailed proof of Theorem 1 can be found in Appendix.

IV. SIMULATION RESULTS

In this section, six sets of simulations are carried out to verify the proposed vehicle side-slip angle estimator. The simulation test is solely carried out on the simulation software of Matlab Simulink and the architecture of simulation implementation is presented in

Figure 3. The simulation parameters are listed in Table 1. The simulation results of simple SMO based on linear tyre model, simple SMO based on non-linear Dugoff tyre model and NS-TSMO based on non-linear Dugoff tyre model are plotted together to compare their estimation performances. In addition to the proposed SMO based on linear and non-linear model, the simulation response of widely used EKF method is also presented here for the comparison. In order to quantitatively compare the simulation results of each method, the root mean square (RMS) values of estimation error of each set of simulations are presented in Table 2.

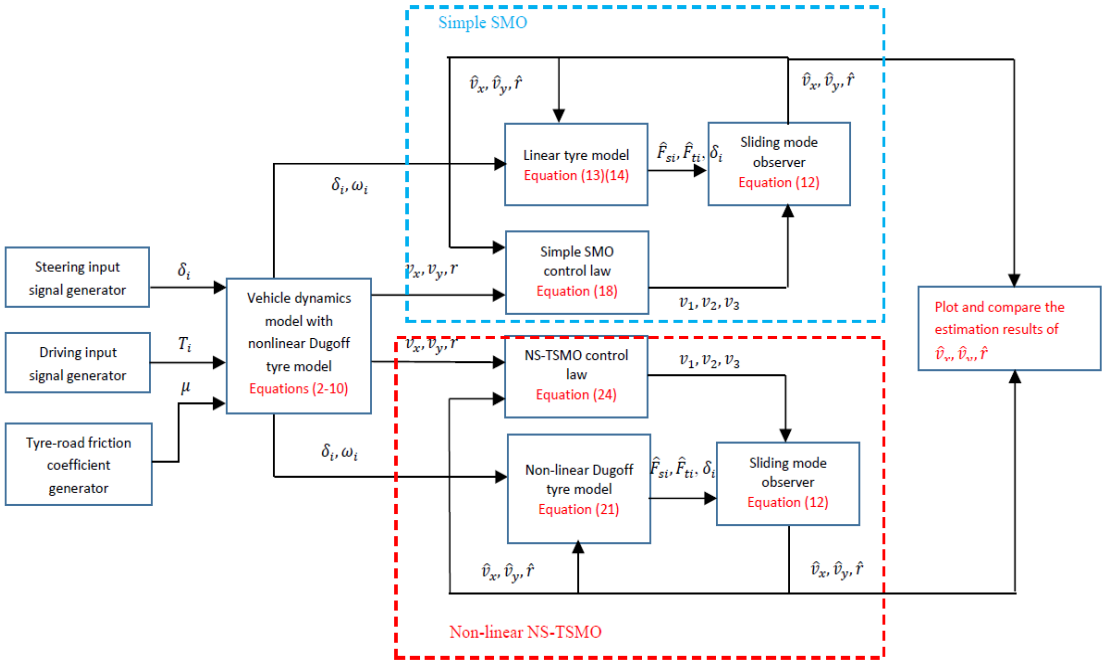

Figure 3. The architecture of the implementation of simulation test on the software of Matlab Simulink

Table 1. Parameter values used in simulations. [26]

m	Mass	1298.9 kg
l_f	Distance of c.g. from the front axle	1 m
l_r	Distance of c.g. from the rear axle	1.454 m
b_f	Front track width	1.436 m
b_r	Rear track width	1.436 m
C_s	Longitudinal stiffness of the tyre	50000 N/unit slip ratio
I_z	Vehicle moment of inertial about yaw axle	1627 kgm^2
R_ω	Wheel radius	0.35 m
I_ω	Wheel moment of inertial	2.1 kgm^2
ε_r	Road adhesion reduction factor	0.015 s/m
C_α	Cornering stiffness of the tyre	30000 N/rad
k_1	Parameter of simple SMO and NS-TSMO	1000
k_2	Parameter of simple SMO	30000

	and NS-TSMO	
k_3	Parameter of simple SMO and NS-TSMO	10000
r_1, r_2, r_3	Parameter of NS-TSMO	250000
$\beta_1, \beta_2, \beta_3$	Parameter of NS-TSMO	1
p_1, p_2, p_3	Parameter of NS-TSMO	6
q_1, q_2, q_3	Parameter of NS-TSMO	4
m_1, m_2, m_3	Parameter of NS-TSMO	10
n_1, n_2, n_3	Parameter of NS-TSMO	12

In the first set of simulations, the vehicle is performing a standard lane change manoeuvre according to [26]. The input steering angle is shown in Figure 4(a) and the measured lateral acceleration is shown in Figure 4(b). The tyre-road friction coefficient is assumed as 0.9 and the vehicle initial velocity is 40 m/s. Figure 4(c), Figure 4(d), and Figure 4(e) show that the simple SMO and NS-TSMO based on non-linear Dugoff tyre model and EKF method can estimate the longitudinal velocity, body slip angle and yaw rate more accurately than linear tyre model estimator. In order to compare the estimation performance of simple SMO and NS-TSMO based on the non-linear tyre model, the sliding mode control gains k_1, k_2, k_3 of these two methods are set as the same values. According to Figure 4(c-e) and RMS values of estimation error in the first

set of simulations in Table 2, the NS-TSMO based on non-linear model can perform better estimation performance than the simple SMO based on non-linear model and EKF method by setting the scaling factors r_1, r_2, r_3 in equation (24) (which is corresponding to the exponential reaching law) as a big value (250000) to achieve fast and finite-time convergence.

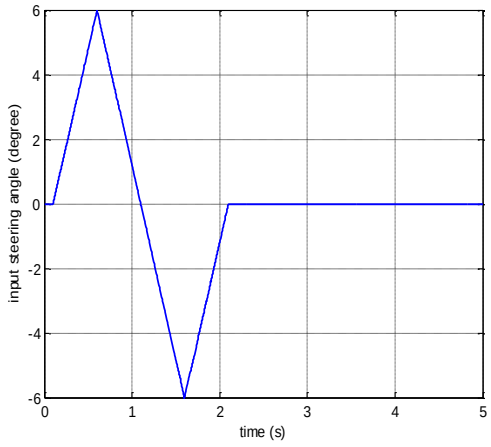

(a)

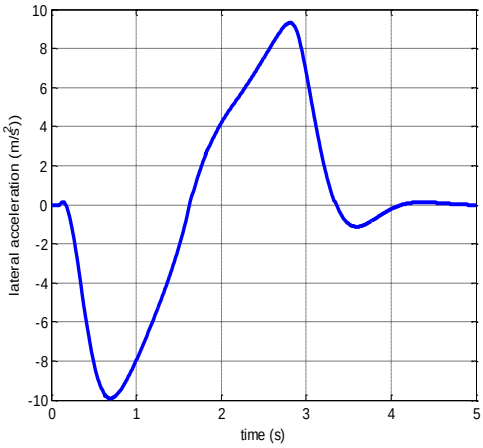

(b)

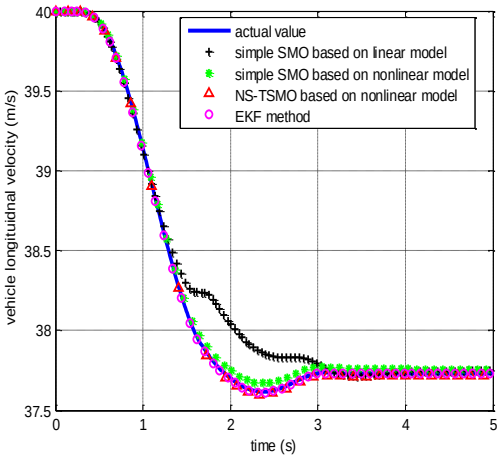
actual value
simple SMO based on linear model
simple SMO based on nonlinear model
NS-TSMO based on nonlinear model
EKF method
vehicle longituidnal velocity (m/s)
time (s)

(c)

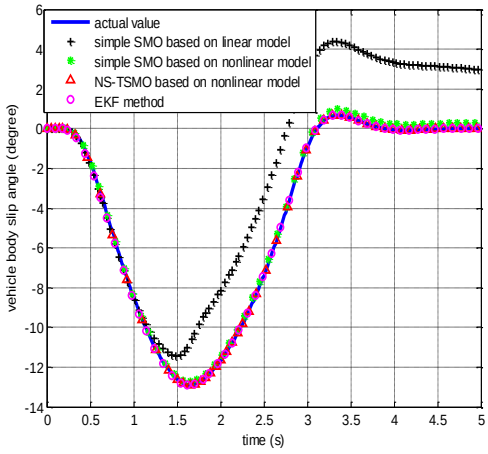
actual value
simple SMO based on linear model
simple SMO based on nonlinear model
NS-TSMO based on nonlinear model
EKF method
vehicle body slip angle (degree)
time (s)

(d)

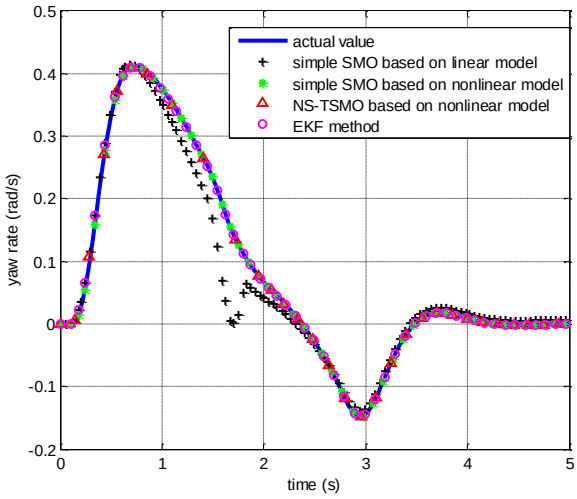
actual value
simple SMO based on linear model
simple SMO based on nonlinear model
NS-TSMO based on nonlinear model
EKF method
yaw rate (rad/s)
time (s)

(e)

Figure 4. Estimation performance in the first set of simulations: (a) input steering angle (b) measured lateral acceleration (c) estimated longitudinal velocity (d) estimated body side-slip angle (e) estimated yaw rate

In the second set of simulations, the initial conditions and input steering angle are the same as the first set of simulations. The measurement value of lateral acceleration is assumed to have the random noise with the variance of 1 (m/s^2) and the zero mean value, which is shown in Figure 5(a). According to Figure 5(b), 5(c) and 5(d), both the simple SMO and the NS-TSMO based on non-linear tyre model show much better estimation performance than simple SMO based on linear tyre model, which shows the advantage of non-linear Dugoff tyre model. The EKF method and the NS-TSMO based on non-linear tyre model show better estimation performance than the simple SMO based on non-linear tyre model, which proves the proposed NS-TSMO and EKF method are robust against the measurement noise with zero mean value. According to RMS values in the second set of simulations in Table 2, the measurement noise affects the estimation results of all the methods, while the proposed NS-TSMO based non-linear model and EKF method shows the best estimation performance.

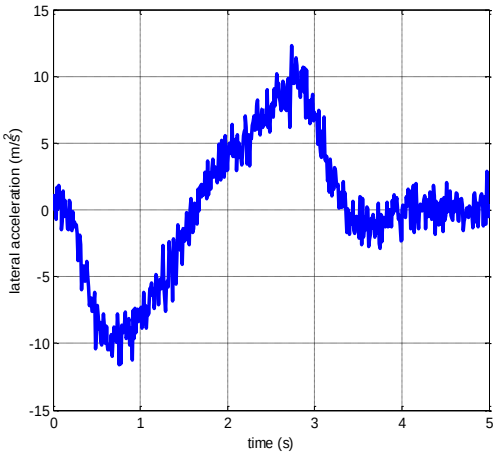
lateral acceleration (m/s^2)
time (s)

(a)

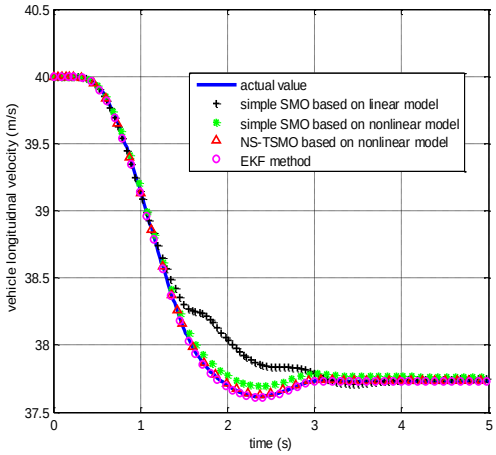
vehicle longitudinal velocity (m/s)
time (s)
actual value
simple SMO based on linear model
simple SMO based on nonlinear model
NS-TSMO based on nonlinear model
EKF method

(b)

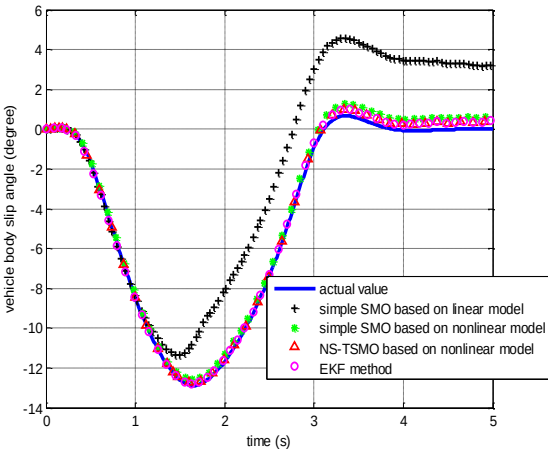
vehicle body slip angle (degree)
time (s)
actual value
simple SMO based on linear model
simple SMO based on nonlinear model
NS-TSMO based on nonlinear model
EKF method

(c)

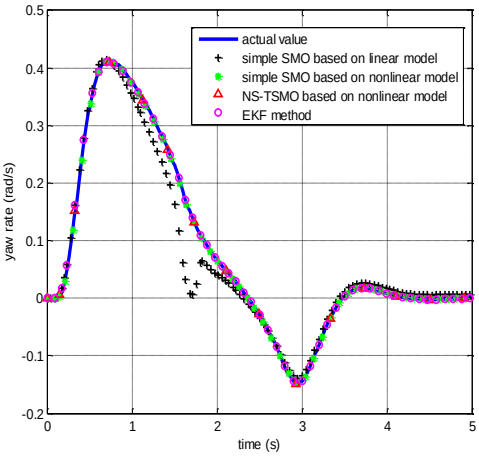
yaw rate (rad/s)
time (s)
actual value
simple SMO based on linear model
simple SMO based on nonlinear model
NS-TSMO based on nonlinear model
EKF method

(d)

Figure 5. Estimation performance in the second set of simulations: (a) measured lateral acceleration (b) estimated longitudinal velocity (c) estimated body side-slip angle (d) estimated yaw rate

In the third set of simulations, the vehicle is performing the J-turn manoeuvre similar to [26]. The input steering angle is shown in Figure 6(a) and the measured lateral acceleration is shown in Figure 6(b). The tyre-road friction coefficient is 0.9 and vehicle initial velocity is still 40 m/s. Figure 6(c), Figure 6(d) and Figure 6(e) clearly present that the estimation results from linear model based estimator have large errors compared with the actual values and the linear based estimation method cannot accurately present the non-linear tyre characteristic. The estimation method of simple SMO and NS-TSMO based on non-linear Dugoff tyre model together with the EKF method, on the other hand, can successfully present the non-linear tyre characteristic and the estimation performance is more attractive. The RMS values of estimation error in third set of simulations in Table 2 suggest that the proposed NS-TSMO based on non-linear model has better estimation performance than simple SMO based on non-linear model and EKF method.

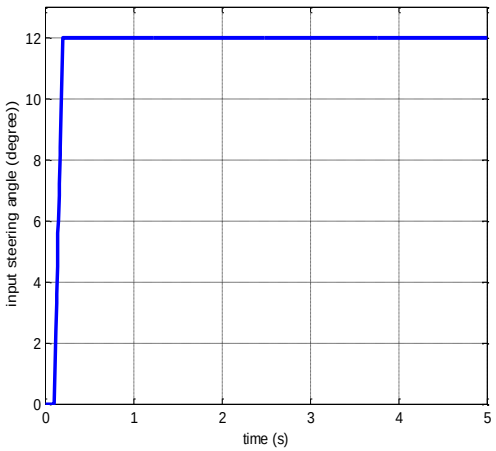
input steering angle (degree))
time (s)

(a)

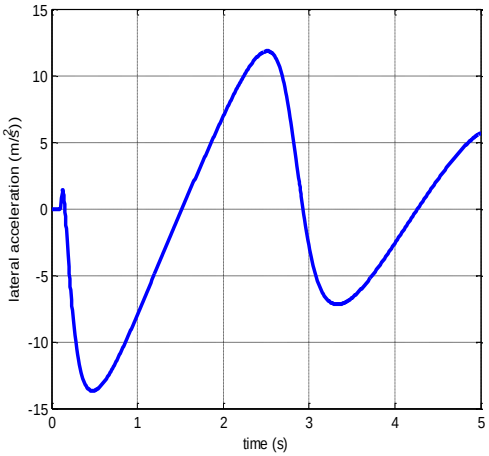
lateral acceleration (m/s2))
time (s)

(b)

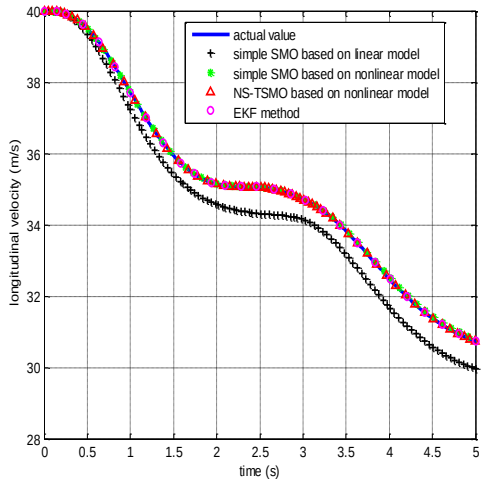
actual value
simple SMO based on linear model
simple SMO based on nonlinear model
NS-TSMO based on nonlinear model
EKF method
longitudinal velocity (m/s)
time (s)

(c)

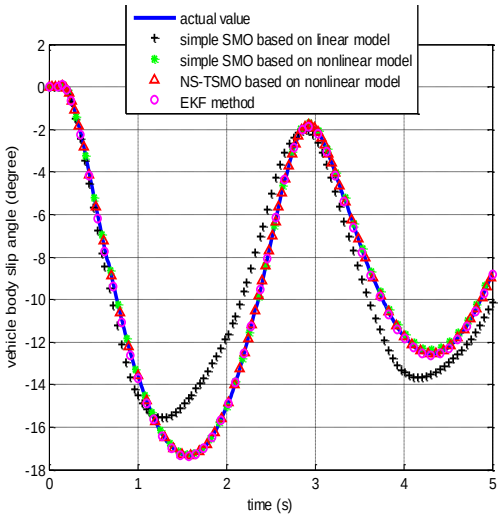
actual value
simple SMO based on linear model
simple SMO based on nonlinear model
NS-TSMO based on nonlinear model
EKF method
vehicle body slip angle (degree)
time (s)

(d)

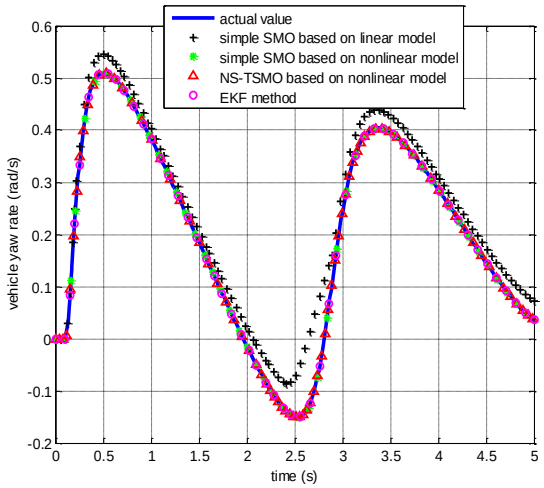

(e)

Figure 6. Estimation performance in the third set of simulations: (a) input steering angle (b) measured lateral acceleration (c) estimated longitudinal velocity (d) estimated body side-slip angle (e) estimated yaw rate

In the fourth set of simulations, the vehicle is performing the J-turn motion with the same input steering angle as Figure 6(a) and the initial velocity is still 40 m/s. The tyre-road friction coefficient is assumed as 0.5 as the vehicle is moving on the slippery road, and all the linear SMO, non-linear SMO and EKF method are assumed to not know this changed friction value and the initial friction coefficient value of 0.9 is still applied on these estimation methods. The measured lateral acceleration is presented in Figure 7(a). Figure 7(b-d) and RMS values in the fourth set of simulations in Table 2 demonstrate that the proposed NS-TSMO based on non-linear tyre model and EKF method can

accurately estimate the vehicle longitudinal velocity and body side-slip angle even when the actual tyre-road friction coefficient is changed. This is because that the estimation error caused by the changed and unidentified friction coefficient is compensated by the feedback measurement values in the NS-TSMO and EKF method. On the other hand, the estimation results of the simple SMO based on linear model are strongly compromised by the changed friction coefficient compared with Figure 6.

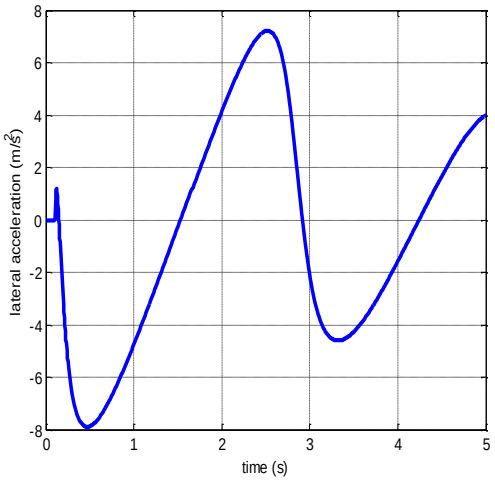

(a)

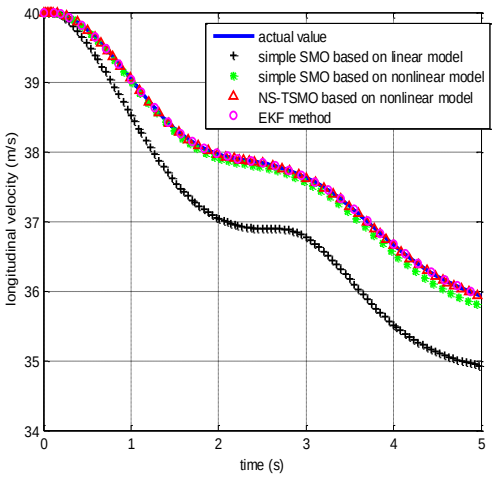

(b)

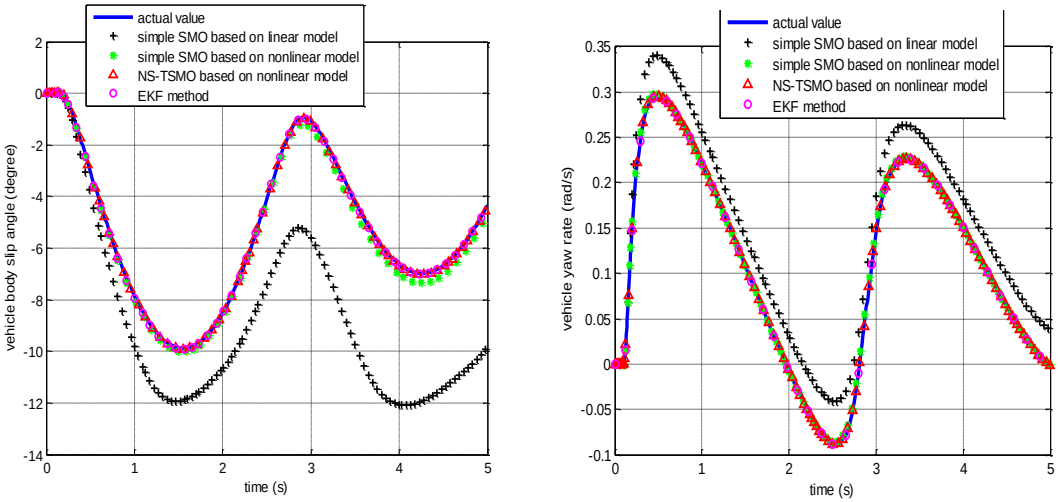

(c) (d)

Figure 7. Estimation performance in the fourth set of simulations: (a) measured lateral acceleration (b) estimated longitudinal velocity (c) estimated body side-slip angle (d) estimated yaw rate

In the fifth set of simulations, all the simulation conditions are the same as the fourth set of simulations except that the cornering stiffness of the non-linear tyre model in the estimator cannot accurately present the actual tyre cornering stiffness and is assumed to be two times larger than the actual value. The default values of cornering stiffness in the estimator is assumed as 30000 N.m and the actual value is 15000 N.m. Figure 8(a) presents the measured lateral acceleration. According to Figure 8 (b-d) and RMS values in the fifth set of simulations in Table 2, the estimation performance of the simple SMO and NS-TSMO based on non-linear tyre model shows a little compromised compared

with Figure 7 (b-d), which is mainly due to the inaccurate cornering stiffness parameter. However, this little compromise of estimation performance can be neglected and the proposed NS-TSMO shows good vehicle state and side-slip angle estimation performance when the tyre parameter is inaccuracy.

In the sixth set of simulations, the vehicle is performing the more challenging sine-wave steering manoeuvre with the input steering angle as Figure 9(a) and the initial velocity is still 40 m/s. In order to further compare the estimation performance between the proposed NS-TSMO and EKF method, the lateral acceleration measurement (Figure 9(b)) has the random noise with the variance of 1 (m/s^2) and the mean value of 0.5 (m/s^2). Compared with measurement noise with the zero mean value in the second set of simulation, the measurement noise with non-zero mean value will significantly impair the estimation performance. According to Figure 9(c-e) and RMS estimation error values in the sixth set of simulations in Table 2, the proposed NS-TSMO based on non-linear tyre model has much better side-slip angle estimation performance than the EKF method. This is because the proposed SMO can overcome the measurement noise by setting the corresponding SMO gain as zero and fully utilise the non-linear vehicle model for the estimation, while the EKF method strongly relies on the measurement value and estimation performance of EKF method is strongly compromised by the measurement noise.

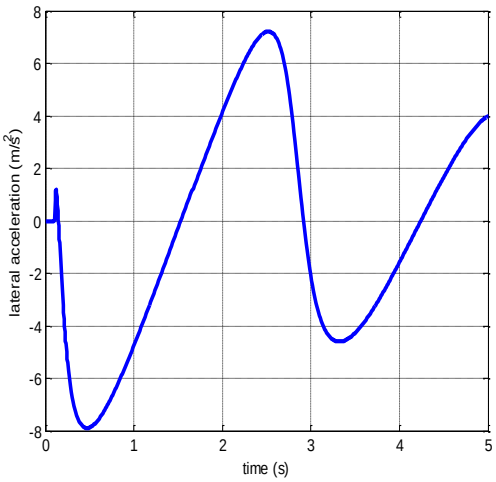
lateral acceleration (m/s2)
time (s)

(a)

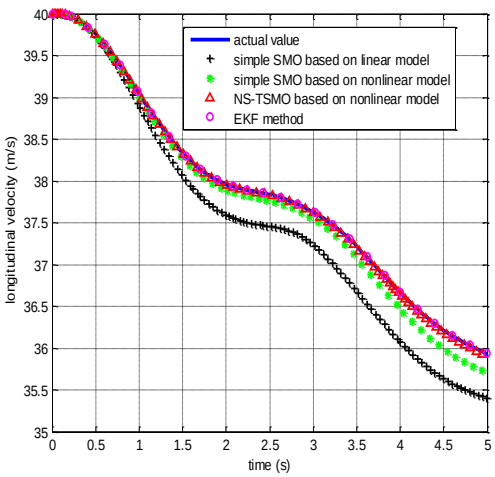
actual value
simple SMO based on linear model
simple SMO based on nonlinear model
NS-TSMO based on nonlinear model
EKF method
longitudinal velocity (m/s)
time (s)

(b)

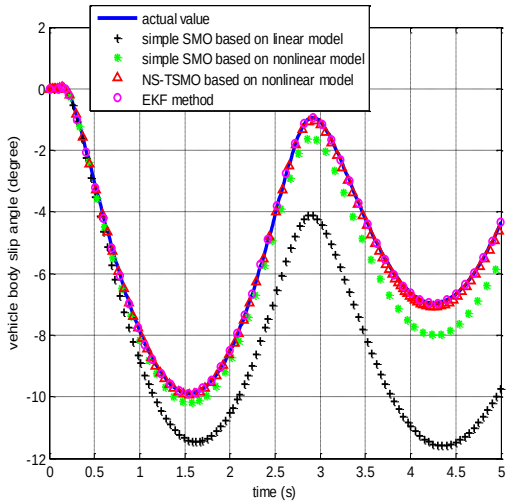
actual value
simple SMO based on linear model
simple SMO based on nonlinear model
NS-TSMO based on nonlinear model
EKF method
vehicle body slip angle (degree)
time (s)

(c)

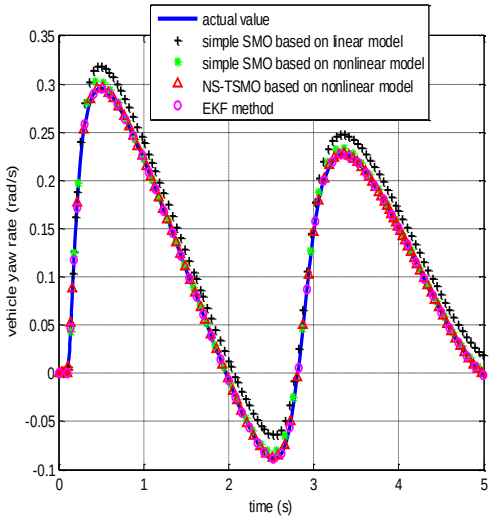
actual value
simple SMO based on linear model
simple SMO based on nonlinear model
NS-TSMO based on nonlinear model
EKF method
vehicle yaw rate (rad/s)
time (s)

(d)

Figure 8. Estimation performance in the fifth set of simulations: (a) measured lateral acceleration (b) estimated longitudinal velocity (c) estimated body side-slip angle (d) estimated yaw rate

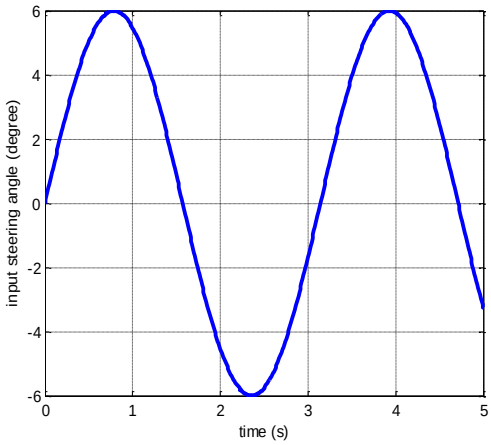

(a)

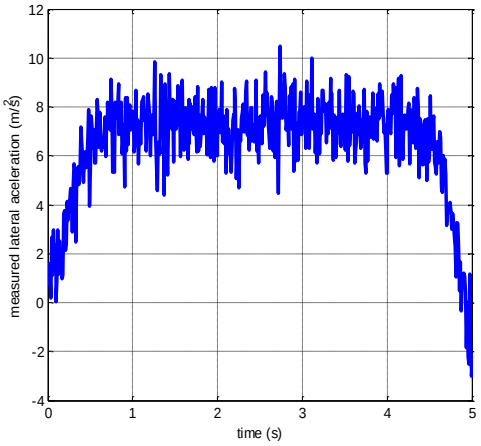

(b)

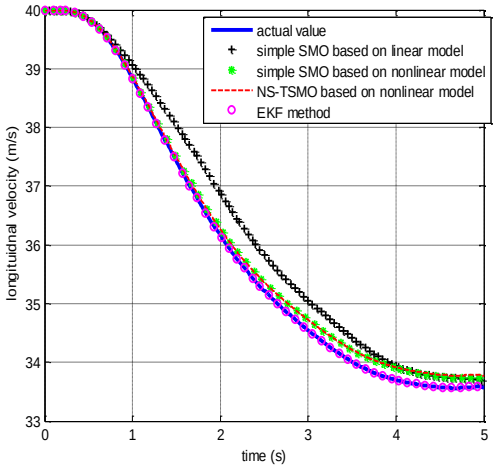

(c)

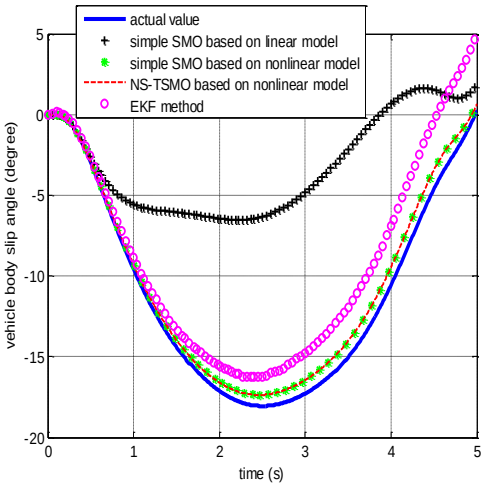

(d)

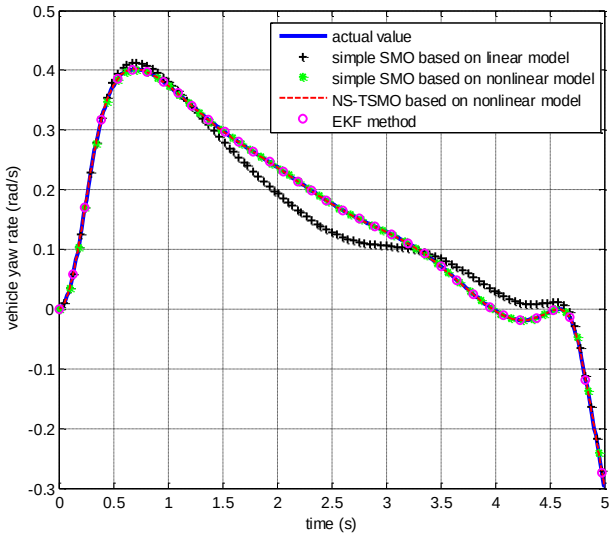

(e)

Figure 9. Estimation performance in the sixth set of simulations: (a) input steering angle (b) measured lateral acceleration (c) estimated longitudinal velocity (d) estimated body side-slip angle (e) estimated yaw rate

Table 2. RMS values of different sets of simulations.

Number of simulation	Longitudinal velocity estimation error (m/s)				Body slip angle estimation error (rad)				Yaw rate estimation error (rad/s)			
	Linear model	Non-linear model		EKF method	Linear model	Non-linear model		EKF method	Linear model	Non-linear model		EKF method
	Simple SMO	Simple SMO	NS-TSMO		Simple SMO	Simple SMO	NS-TSMO		Simple SMO	simple SMO	NS-TSMO	
1	0.1621	0.0301	0.0034	0.0239	0.0502	0.0038	3.05	6.056	0.0348	0.0018	1.548	5.41

							41 × 10^{-4}	1 × 10^{-4}			× 10^{-4}	29× 10^{-4}
2	0.1638	0.0450	0.0212	0.0215	0.0519	0.0072	0.0037	0.0037	0.0338	0.0019	1.8622 × 10^{-4}	5.4186 × 10^{-4}
3	0.6035	0.0300	0.0031	0.0383	0.0291	0.0030	2.0131 × 10^{-4}	0.0016	0.0432	0.0019	2.056 × 10^{-4}	0.0014
4	0.8523	0.0832	0.0060	0.0032	0.0642	0.0044	5.531 × 10^{-4}	9.2883 × 10^{-4}	0.037	0.0036	5.1597 × 10^{-4}	7.691 × 10^{-5}
5	0.3985	0.1396	0.0141	0.0035	0.0526	0.0114	0.0013	6.8864 × 10^{-4}	0.0193	0.0053	7.4481 × 10^{-4}	4.6665 × 10^{-5}
6	0.4291	0.1416	0.1213	0.0059	0.1571	0.013	0.0105	0.0441	0.0259	5.1541 × 10^{-4}	3.0972 × 10^{-5}	4.3880 × 10^{-5}

V. CONCLUSION

This paper proposes an innovative side-slip angle estimator based on the non-linear Dugoff tyre model and non-singular terminal sliding mode technique. Based on the simulation results and compared with the simple SMO based on linear tyre model and non-linear tyre model and EKF estimation method, the major findings can be summarized as follows:

1) The proposed simple SMO and NS-TSMO based on non-linear tyre model can achieve much better estimation performance than the simple SMO based on linear tyre model in all the six sets of simulations, which proves the advantageous of the including the non-linear Dugoff tyre model into the side-slip angle estimator.

2) The proposed NS-TSMO based on non-linear tyre model can achieve better estimation performance than the simple SMO based on non-linear tyre model in all the simulations, which proves the NS-TSMO can achieve fast and finite-time convergence and is advantageous over the simple SMO.

3) When the measurement noise of lateral acceleration exists, the proposed NS-TSMO can better overcome the measurement noise and achieve the fast convergence compared with the simple SMO based on linear and non-linear tyre model, while the EKF method can only achieve the good estimation performance when the measurement noise has zero mean value.

4) When the proposed non-linear tyre model based observer do not know the change of actual tyre-road friction condition or the tyre model has inaccurate parameters, simulation results have proved that the proposed NS-TSMO is quite robust against the parameter error and friction coefficient change and shows good estimation performance of vehicle state and side-slip angle.

In the future, the experiment should be carried out to validate the proposed side-slip angle observer.

Appendix

Proof of Theorem 1:

(1) Defined the Lyapunov function as $V_3 = \frac{1}{2}s_3^2$, and the time derivative of V_3 can be obtained as:

$$\begin{aligned}\dot{V}_3 = s_3\dot{s}_3 = s_3\Big[&-\left(k_3 s_3 + r_3 s_3^{m_3/n_3}\right)\tilde{r}^{p_3/q_3-1} \\ &+ \frac{p_3}{\beta_3 q_3}\tilde{r}^{p_3/q_3-1}\left(B_{y3}(\delta_i)\boldsymbol{F_s} + B_{x3}(\delta_i)\boldsymbol{F_t}\right)\Big] \\ &= \left(-k_3 s_3^2 - r_3 s_3^{m_3/n_3+1} + \frac{p_3 s_3}{\beta_3 q_3}\left(B_{y3}(\delta_i)\boldsymbol{F_s} + B_{x3}(\delta_i)\boldsymbol{F_t}\right)\right)\tilde{r}^{p_3/q_3-1}\end{aligned}$$

(A1)

When (27c) is satisfied:

if $s_3 > 0, \frac{p_3 s_3}{\beta_3 q_3}\left(B_{y3}(\delta_i)\boldsymbol{F_s} + B_{x3}(\delta_i)\boldsymbol{F_t}\right) < s_3 c_3$

$$\dot{V}_3 < s_3\left(-k_3 s_3 - r_3 s_3^{m_3/n_3} + c_3\right)\tilde{r}^{p_3/q_3-1} < -r_3 s_3^{m_3/n_3+1}\tilde{r}^{p_3/q_3-1} < 0$$

(A2a)

if $s_3 < 0, \frac{p_3 s_3}{\beta_3 q_3}\left[B_{y3}(\delta_i)\boldsymbol{F_s} + B_{x3}(\delta_i)\boldsymbol{F_t}\right] < -s_3 c_3$

$$\dot{V}_3 < s_3\left(-k_3 s_3 - r_3 s_3^{m_3/n_3} - c_3\right)\tilde{r}^{p_3/q_3-1} < -r_3 s_3^{m_3/n_3+1}\tilde{r}^{p_3/q_3-1} < 0$$

(A2b)

if $s_3 = 0, \tilde{r} \to 0$.

Thus, when (27c) is satisfied, equation (A2) is obtained and $\dot{V}_3 < 0$ is proved. And hence, the yaw rate estimation error $\tilde{r}$ will converge to zero ultimately.

(2) Defined the Lyapunov function as $V_1 = \frac{1}{2}s_1^2$, and the time derivative of V_1 can be obtained as:

$$\dot{V}_1 = s_1\dot{s}_1 = -s_1\left(k_1 s_1 + r_1 s_1^{m_1/n_1}\right)\left(\int \tilde{a}_x\right)^{\frac{p_1}{q_1}-1} + \frac{p_1 s_1}{\beta_1 q_1}\left(\int \tilde{a}_x\right)^{\frac{p_1}{q_1}-1}\left[\dot{\tilde{v}}_x - \left(\tilde{v}_y r + \hat{v}_y \tilde{r}\right)\right] \tag{A3}$$

when (27a) is satisfied

if $s_1 > 0$, $\frac{p_1 s_1}{\beta_1 q_1}\left[\dot{\tilde{v}}_x - \left(\tilde{v}_y r + \hat{v}_y \tilde{r}\right)\right] = \frac{p_1 s_1}{\beta_1 q_1}\left[B_{y1}(\delta_i)\Delta \boldsymbol{F_s} + B_{x1}(\delta_i)\Delta \boldsymbol{F_t}\right] < s_1 c_1$

$$\dot{V}_1 < s_1\left(-k_1 s_1 - r_1 s_1^{m_1/n_1} + c_1\right)\left(\int \tilde{a}_x\right)^{\frac{p_1}{q_1}-1} < -r_1 s_1^{m_1/n_1+1}\left(\int \tilde{a}_x\right)^{\frac{p_1}{q_1}-1} < 0 \tag{A4a}$$

if $s_1 < 0$, $\frac{p_1 s_1}{\beta_1 q_1}\left[\dot{\tilde{v}}_x - \left(\tilde{v}_y r + \hat{v}_y \tilde{r}\right)\right] = \frac{p_1 s_1}{\beta_1 q_1}\left[B_{y1}(\delta_i)\Delta \boldsymbol{F_s} + B_{x1}(\delta_i)\Delta \boldsymbol{F_t}\right] < -s_1 c_1$

$$\dot{V}_1 < s_1\left(-k_1 s_1 - r_1 s_1^{m_1/n_1} - c_1\right)\left(\int \tilde{a}_x\right)^{\frac{p_1}{q_1}-1} < -r_1 s_1^{m_1/n_1+1}\left(\int \tilde{a}_x\right)^{\frac{p_1}{q_1}-1} < 0 \tag{A4b}$$

if $s_1 = 0$, $\tilde{v}_x \to 0$.

When (27a) is satisfied, equation (A4) is obtained and $\dot{V}_1 < 0$ is proved. Thus, the longitudinal velocity estimation error $\tilde{v}_x$ will converge to zero ultimately.

(3) Defined the Lyapunov function as $V_2 = \frac{1}{2}s_2^2$, and the time derivative of V_2 can be obtained as:

$$\begin{aligned}\dot{V}_2 &= s_2\dot{s}_2 = s_2\dot{s}_2 \\ &= -s_2\left(k_2 s_2 + r_2 s_2^{m_2/n_2}\right)\left(\int \tilde{a}_y\right)^{\frac{p_2}{q_2}-1} \\ &+ \frac{p_2 s_2}{\beta_2 q_2}\left(\int \tilde{a}_y\right)^{\frac{p_2}{q_2}-1}\left[\dot{\tilde{v}}_y + (\tilde{v}_x r + \hat{v}_x \tilde{r})\right]\end{aligned} \tag{A5}$$

When (27b) is satisfied

if $s_2 > 0, \frac{p_2 s_2}{\beta_2 q_2}\left[\dot{\tilde{v}}_y + (\tilde{v}_x r + \hat{v}_x \tilde{r})\right] = \frac{p_2 s_2}{\beta_2 q_2}\left[B_{y2}(\delta_i)\Delta \boldsymbol{F_s} + B_{x2}(\delta_i)\Delta \boldsymbol{F_t}\right] < s_2 c_2$

$$\dot{V}_2 < s_2\left(-k_2 s_2 - r_2 s_2^{m_2/n_2} + c_2\right)\left(\int \tilde{a}_y\right)^{\frac{p_2}{q_2}-1} < -r_2 s_2^{m_2/n_2+1}\left(\int \tilde{a}_y\right)^{\frac{p_2}{q_2}-1} < 0 \tag{A6a}$$

if $s_2 > 0, \frac{p_2 s_2}{\beta_2 q_2}\left[\dot{\tilde{v}}_y + (\tilde{v}_x r + \hat{v}_x \tilde{r})\right] = \frac{p_2 s_2}{\beta_2 q_2}\left[B_{y2}(\delta_i)\Delta \boldsymbol{F_s} + B_{x2}(\delta_i)\Delta \boldsymbol{F_t}\right] < -s_2 c_2$

$$\dot{V}_2 < s_2\left(-k_2 s_2 - r_2 s_2^{m_2/n_2} - c_2\right)\left(\int \tilde{a}_y\right)^{\frac{p_2}{q_2}-1} < -r_2 s_2^{m_2/n_2+1}\left(\int \tilde{a}_y\right)^{\frac{p_2}{q_2}-1} < 0 \tag{A6b}$$

if $s_2 = 0$, $\tilde{v}_y \to 0$.

When (27b) is satisfied, equation (A6) are obtained and $\dot{V}_2 < 0$ is proved.

Thus, the longitudinal velocity estimation error $\tilde{v}_y$ will converge to zero ultimately.

Acknowledgement

This research was supported under Australian Research Council's Discovery Projects funding scheme (project number DP140100303) and the Open Research Fund Program of the State Key Laboratory of Advanced Design and Manufacturing for Vehicle Body, Hunan University (31515001).

References

[1] van Zanten AT. Bosch ESP systems: 5 year of experience. SAE, Warrendale, PA, 2000-01-1633.

[2] Wu J, Cheng S, Liu B and Liu C. A Human-Machine-Cooperative-Driving Controller based on AFS and DYC for vehicle dynamic stability. *Energies*; 2017; 10(1737):1-18.

[3] Li L, Jia G, Ran X, Song J and Wu K. A variable structure extended Kalman filter for vehicle sideslip angle estimation on a low friction road. *Vehicle System Dynamics* 2014; 52: 280-308.

[4] Li L, Yang K, Jia G, Ran X, Song J and Han Z. Comprehensive tyre–road friction coefficient estimation based on signal fusion method under complex maneuvering operations. *Mechanical System and Signal Processing* 2015; 56:259-276.

[5] Zhang L, Li L, Lin C, Wang C, Qi B and Song J. Coaxialcoupling coupling traction control for a four-wheel-independent-drive electric vehicle on a complex road. *PIMech Eng D-J Aut* 2014; 228(12):1398-1414.

[6] Chen Y and Wang J. Design and experimental evaluations on energy efficient control allocation methods for overactuated electric vehicles: Longitudinal motion case. *IEEE Transactions on Mechatronics* 2014; 19(2): 538-548.

[7] de Castro R, Tanelli M, Araújo R and Savaresi S. Design of safety-oriented control allocation strategies for overactuated electric vehicles. *Vehicle System Dynamics* 2014; 52(8): 1017-1046.

[8] Ray LR. Non-linear state and tyre force estimation for advanced vehicle control. *IEEE Trans. Control Syst. Technol.* 1995; 3(1): 117-124.

[9] Ray L. Non-linear tyre force estimation and road friction identification: simulation and experiments. *Automatica* 1997; 33(10): 1819-1833.

[10] Hiemer H, v. Vietinghoff A, Kiencke U and Matsunaga T. Determination of the vehicle body side slip angle with non-linear observer strategies. SAE, Warrendale, PA, 2005.

[11] Jiang G, Liu L, Guo C, Chen J, Muhammad F and Miao X. A novel fusion algorithm for estimation of the side-slip angle and the rolling angle of a vehicle with optimized key parameters. *Proc IMechE Part D: J Automobile Engineering* 2017; 231(2): 161-174.

[12] Best MC, Gordon TJ and Dixon PJ. An extended adaptive Kalman filter for real-time state estimation of vehicle handing dynamics. *Vehicle System Dynamics* 2000; 34(1): 57-75.

[13] Best MC, Newton AP and TuplinS. The identifying extended Kalman filter: parametric system identification of a vehicle handling model. *Proc. IMechE Part K: J. Multi-body Dynamics* 2007; 221: 87-98.

[14] Cheng S, Li L and Chen J. Fusion Algorithm Design Based on Adaptive SCKF and Integral Correction for Side-Slip Angle Observation. *IEEE Transactions on Industrial Electronics* 2018; 65(7): 5754-5763.

[15] Zhang H, Zhang G and Wang J. H∞ Observer Design for LPV Systems With Uncertain Measurements on Scheduling Variables: Application to an Electric Ground Vehicle. *IEEE/ASME Transactions on Mechatronics* 2016; 21(3): 1659-1670.

[16] Zhang H and Wang J. Active Steering Actuator Fault Detection for an Automatically-Steered Electric Ground Vehicle. *IEEE Transactions on Vehicular Technology* 2017; 66(5): 3685-3702.

[17] Stephant J, Charara A and Meizel D. Virtual sensor: Application to vehicle sideslip angle and transversal forces. *IEEE Transactions on industrial electronics* 2004; 51(2): 278-289.

[18] Zhao LH, Liu ZY and Chen H. Design of a Non-linear Observer for Vehicle Velocity Estimation and Experiments. *IEEE Transactions on Control Systems Technology* 2011; 19(3): 664-672.

[19] Huang G, Saratchandran P and Sundararajan N. A generalized growing and pruning RBF (GGAP-RBF) neural network for function approximation. *IEEE Transactions on Neural Network* 2005, 16(1): 57-67.

[20] Shi S, Lupker H, Bremmer P and Zuurbier J. Estimation of Vehicle side slip angle based on fuzzy logic. *Automotive Engineering* 2005; 4:426-430.

[21] Zhang H, Zhang G and Wang J. Sideslip Angle Estimation of an Electric Ground Vehicle via Finite-Frequency H∞ Approach. *IEEE Transactions on Transportation Electrification* 2016; 2(2): 200-209.

[22] Pacejka HB and Bakker E. The Magic Formula Tyre Model. *Vehicle System Dynamics* 1992; 21(S1): 1-18.

[23] Deur J, Kranjčević N, Hofmann O, Asgari J and Hrovat D. Analysis of Lateral Tyre Friction Dynamics. *Vehicle System Dynamics* 2009; 47(7): 831-850.

[24] Uil T. Tyre models for steady-state vehicle handling analysis. Master's Thesis, Eindhoven University of Technology, Department of Mechanical Engineering, Dynamics and Control Group, Eindhoven, 2007.

[25] Dugoff H, Fancher P and Segel L. An Analysis of Tyre Traction Properties and Their Influence on Vehicle Dynamic Performance. in *SAE Technical Paper 700377*, 1970.

[26] Boada BL, Boada MJL and Diaz V. Fuzzy-logic applied to yaw moment control for vehicle stability. *Vehicle System Dynamics* 2005, 43(10): 753-770.

[27] Li B, Du H and Li W. A Potential Field Approach-Based Trajectory Control for Autonomous Electric Vehicles With In-Wheel Motors. *IEEE Transactions on Intelligent Transportation Systems* 2017; 18(8): 2044-2055.

[28] Li B, Du H and Li W. Fault-tolerant control of electric vehicles with in-wheel motors using actuator-grouping sliding mode controllers. *Mechanical Systems and Signal Processing* 2015; 72-73: 462-485.

[29] Ma B, Liu Y, Gao Y, Yang Y, Ji X and Bo Y. Estimation of vehicle sideslip angle based on steering torque. *Int J Adv Manuf Technol* 2018; 94: 3229-3237.

[30] Li J and Zhang J. Vehicle Sideslip Angle Estimation Based on Hybrid Kalman Filter. *Mathematical Problems in Engineering* 2016; 2016:1-10.

[31] Hsu YJ, Laws S, Gadda CD and Gerdes JC. A method to estimate the friction coefficient and tyre slip angle using steering torque. in *Proceedings of 2006 ASME international mechanical engineering congress and exposition*, Chicago, Illinois, USA, 2006.

[32] Hsu YJ, Laws S and Gerdes JC. Estimation of tyre slip angle and friction limits using steering torque. *IEEE Trans Control Syst Technol* 2010; 18(4):896-907.

[33] Doumiati M, Victorino AC, Charara A and Lechner D. Onboard real-time estimation of vehicle lateral tyre–road forces and sideslip angle. *IEEE/ASME Transactions on Mechatronics* 2011; 16(4): 601-614.

[34] Kachroo P and Tomizuka M. Chattering reduction and error convergence in the sliding mode control of a class of non-linear systems, *IEEE Trans. Autom. Control* 1996; 41(7): 1063-1068.

[35] Gao W and Hung JC. Variable structure control of non-linear systems: a new approach. *IEEE Trans. Ind. Electron.* 1993; 40(1):45-55.

[36] Zong Q, Zhao ZS and Zhang J. Higher order sliding mode control with self-tuning law based on integral sliding mode. *IET Control Theory Appl.* 2010; 4(7): 1282-1289.

[37] Alipour H, Sharifian MBB and Sabahi M. A Modified Integral Sliding Mode Control to Lateral Stabilisation of 4-Wheel Independent drive electric vehicles. *Vehicle System Dynamics* 2014; 52(12): 1584-1606.

[38] Guo J, Luo Y and Li K. Dynamic coordinated control for over-actuated autonomous electric vehicles with nonholonomic constraints via nonsingular terminal sliding mode technique. *Non-linear Dynamics* 2016; 85: 583-597.

[39] Zhao Y and Zhang J. Yaw stability control of a four-independent-wheel drive electric vehicle. *Int. J. Electric and Hybrid Vehicles* 2009; 2(1): 64-76.